

# Paleostress analysis of the Nyasa / Malawi Rift: implication for the present-day regional dynamics

Athanas Simon MACHEYEKI<sup>1</sup> and Hassan Mdala<sup>2</sup>

<sup>1</sup>University of Dodoma

<sup>2</sup>Geological Survey of Malawi

December 22, 2022

## Abstract

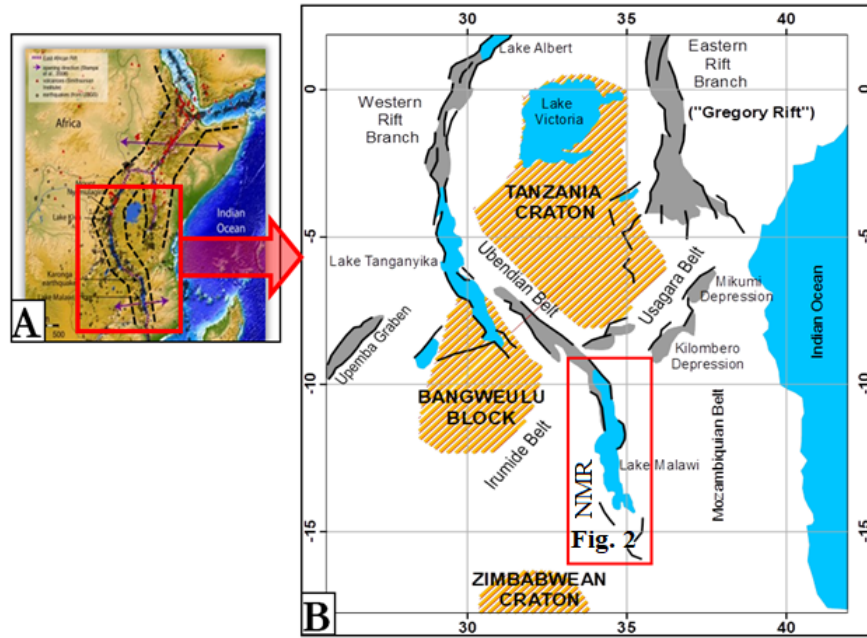
The Nyasa/ Malawi rift is characterized by poor magma with relatively large earthquakes. There has been a controversy as to the stress kinematics of the rift, some considering it as part of the transform fault and some considering it as a rift structure characterized by normal faulting. To review this controversy, we collect fault slip data from the central to the southern end of the rift and integrate our results with published focal mechanisms fault slip data on the rift. Results show that the central part of the rift is under radial extension whereas the southern half is under oblique NNE-SSW transtensive tectonic regime with the horizontal axis of minimum extension = 020°. Further south, the obliquity extension rotates by about 15° reaching N-S with Shmin = 175°. The level of structural penetration and intensity of faulting show that the N-S opening is more important and prominent in the south than towards the north. We also find that the faults that dip to the east and trending NW-SE are characterized by sinistral sense of movement whereas those that dip to the southwestern side are characterized by dextral sense of movements. This implies that regionally, the rift is essentially under normal faulting regime but with a significant strike –slip component – hence the obliquity kinematics. Tectonic regimes obtained from fault-slip data are related to lithospheric scale and involve both the crust and the upper mantle. Thus, the pure NNW-SSE extension related to focal mechanism data are crust deformation related events.

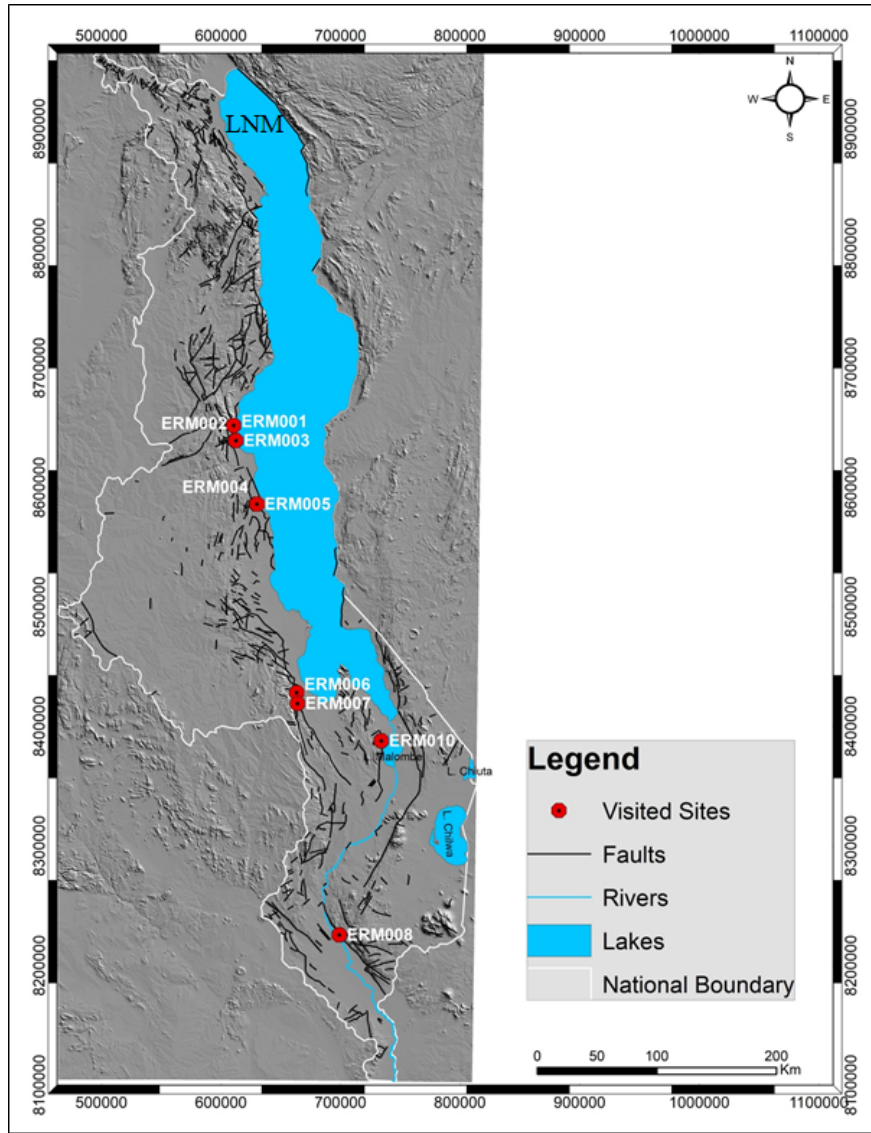
## Hosted file

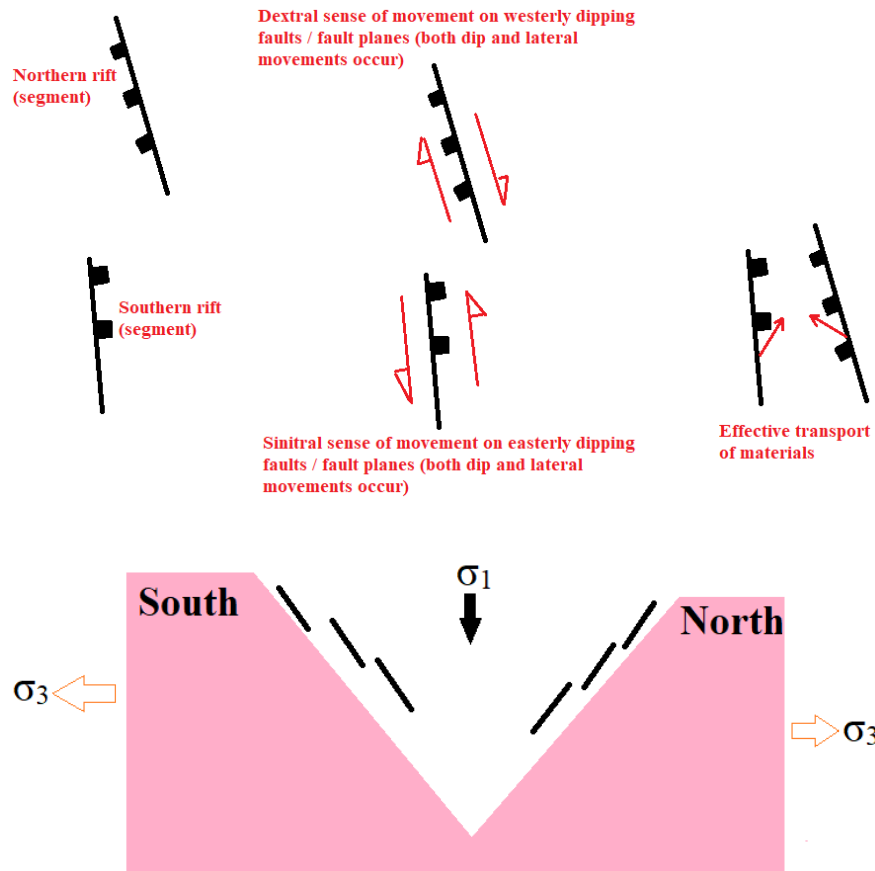
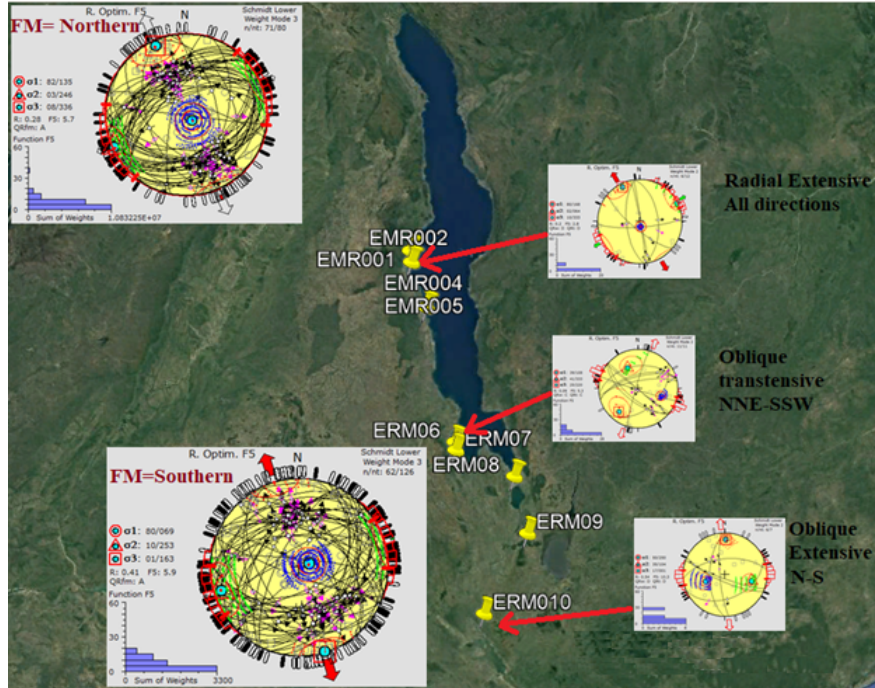
951450\_0\_art\_file\_10507065\_rmflyb.docx available at <https://authorea.com/users/568955/articles/614569-paleostress-analysis-of-the-nyasa-malawi-rift-implication-for-the-present-day-regional-dynamics>

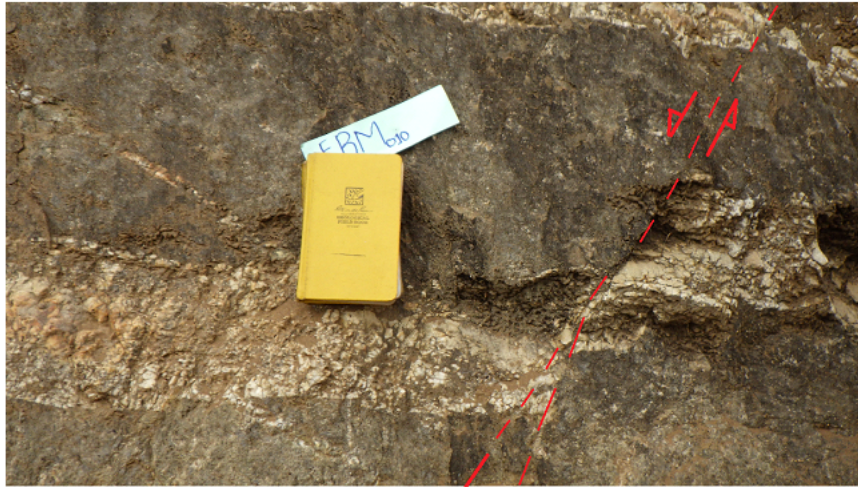
## Hosted file

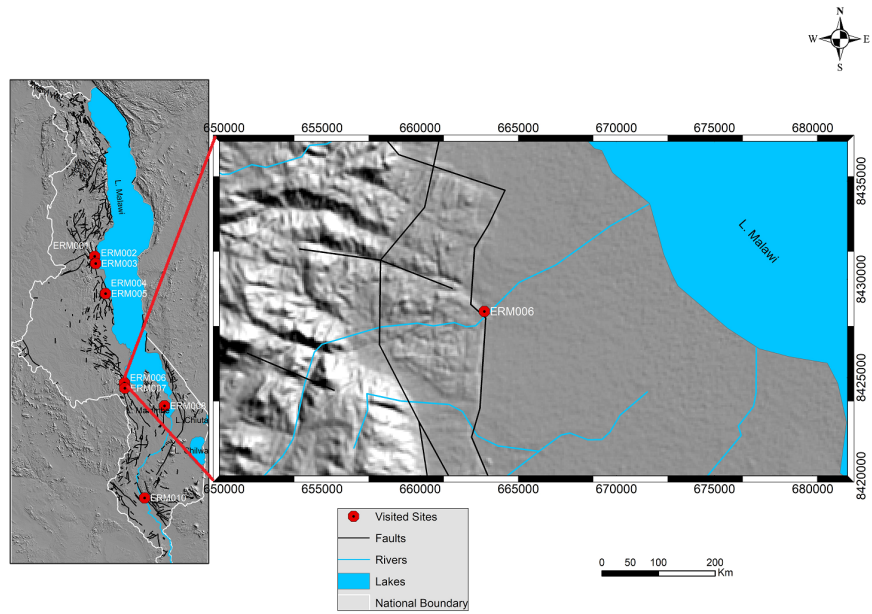
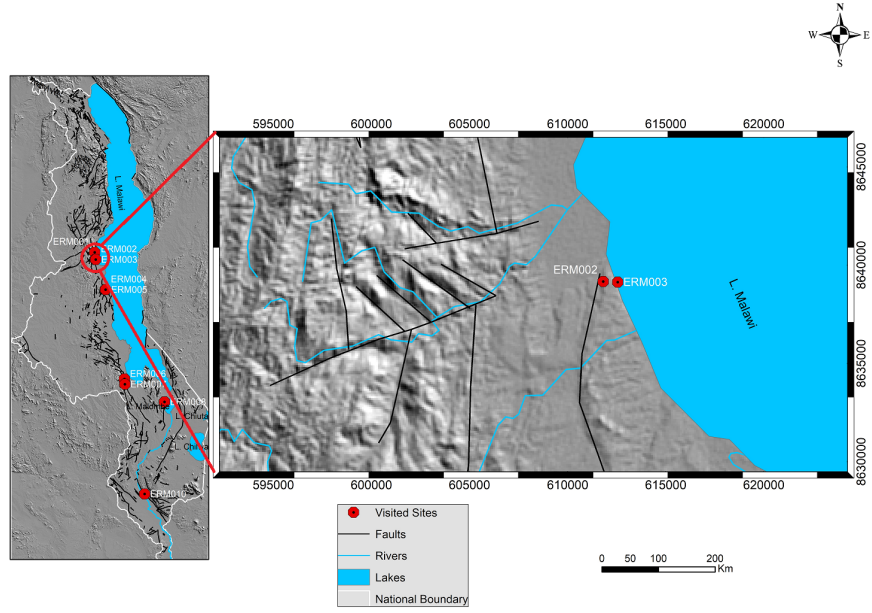
951450\_0\_table\_10507078\_rmflyr.docx available at <https://authorea.com/users/568955/articles/614569-paleostress-analysis-of-the-nyasa-malawi-rift-implication-for-the-present-day-regional-dynamics>

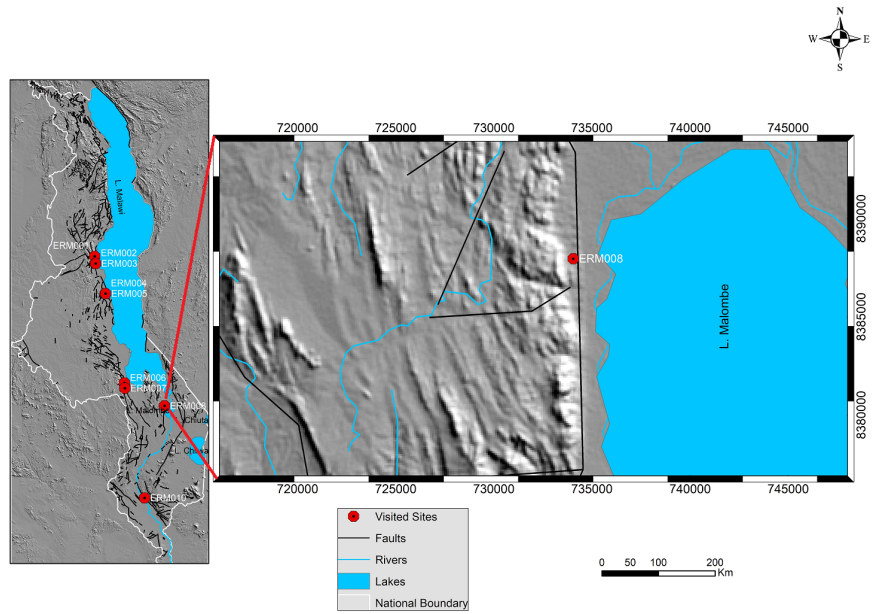
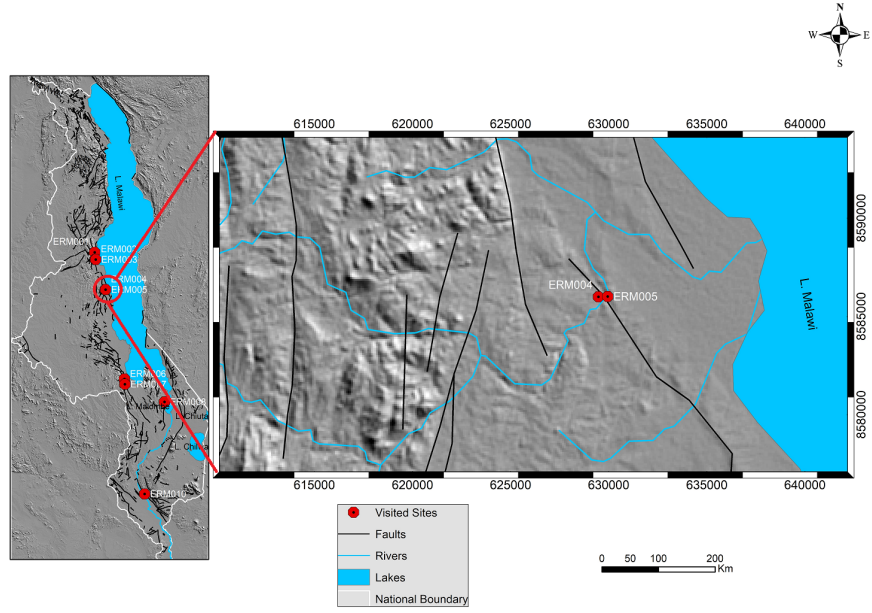


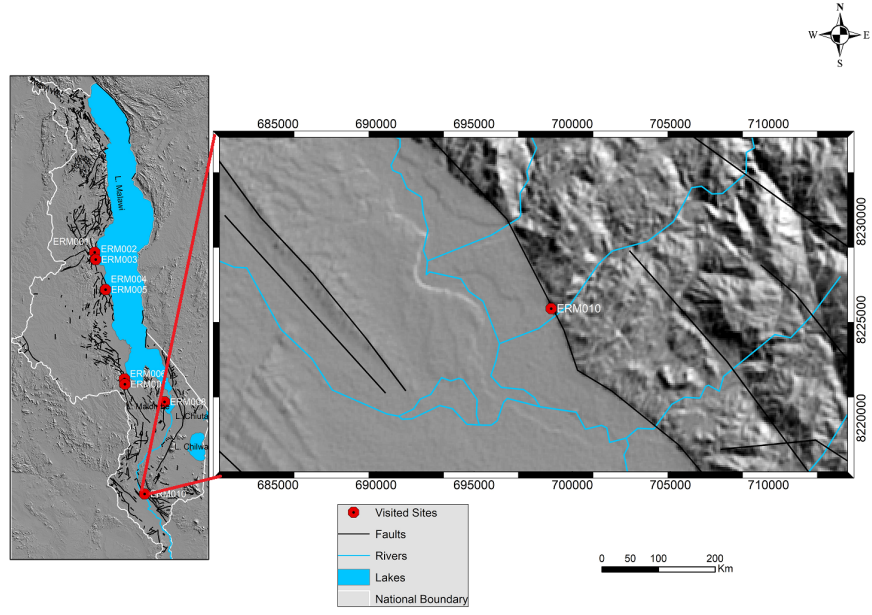












1 **Paleostress analysis of the Nyasa / Malawi Rift: implication for the present-**  
2 **day regional dynamics**

3

4 Athanas S. Macheyeke<sup>(1,2)</sup> and Hassan Mdala<sup>(3)</sup>

5 <sup>(1)</sup>Department of Geology, College of Earth Sciences and Engineering, the University of Dodoma-  
6 Tanzania

7 [asmacheyeke@yahoo.com](mailto:asmacheyeke@yahoo.com)

8 <sup>(2)</sup>Earth Sciences Institute of Shinyanga, P. O. Box 1016, Shinyanga-Tanzania

9 <sup>(3)</sup>Geological Survey Department of Malawi, Regional Office North, Pvt Bag 9, Mzuzu, Malawi

10

11 **Abstract**

12 The Nyasa/ Malawi rift is characterized by poor magma with relatively large earthquakes. There  
13 has been a controversy as to the stress kinematics of the rift, some considering it as part of the  
14 transform fault and some considering it as a rift structure characterized by normal faulting. To  
15 review this controversy, we collect fault slip data from the central to the southern end of the rift  
16 and integrate our results with published focal mechanisms fault slip data on the rift. Results show  
17 that the central part of the rift is under radial extension whereas the southern half is under  
18 oblique NNE-SSW transtensive tectonic regime with the horizontal axis of minimum extension =  
19 020°. Further south, the obliquity extension rotates by about 15° reaching N-S with  $Sh_{min} =$   
20 175°. The level of structural penetration and intensity of faulting show that the N-S opening is  
21 more important and prominent in the south than towards the north. We also find that the faults

22 that dip to the east and trending NW-SE are characterized by sinistral sense of movement  
23 whereas those that dip to the southwestern side are characterized by dextral sense of movements.  
24 This implies that regionally, the rift is essentially under normal faulting regime but with a  
25 significant strike –slip component – hence the obliquity kinematics. Tectonic regimes obtained  
26 from fault-slip data are related to lithospheric scale and involve both the crust and the upper  
27 mantle. Thus, the pure NNW-SSE extension related to focal mechanism data are crust  
28 deformation related events.

29

30 **Key words:** Nyasa / Malawi rift, East African Rift system, Paleostress analysis, Oblique  
31 transtensive rifting, radial extension, stress perturbation

32

### 33 **Introduction**

34 There are various models of rifting, major ones attest to active rifting and passive rifting (e.g.  
35 Bott, 1995; Prodehl et al., 1997; Corti et al., 2003). In the first case magma is the source of  
36 rifting where underlying magma heats the bottom of the lithosphere or the crust causing it to  
37 expand and consequently thin away and eventually leading to rifting (Buck, 1991; Bott, 1995;  
38 Gueydan et al., 2014). In the second case, no magma is involved in the rifting process (Bott,  
39 2006; Hao et al., 2020) but that the rifting is caused by far-field stresses. There are times where  
40 both models operate (e.g. Dumond et al., 2017; Ebinger, 2020)

41 The East African Rift System (EARS) is one of such lithospheric scale structures whereby rifting  
42 occurs through active and passive models (e.g. Bott, 1995; Corti et al., 2003). In the process of  
43 rifting, earthquakes of various sizes occur depending on the source of the driving stresses and the

44 magnitude (s) of the same. Usually, deep seated earthquakes cause large to major earthquakes in  
45 rift systems. The largest recorded earthquake in rift systems are in little excess of Mw 7 ((e.g.  
46 Yan and Chen, 2010). In the EARS, the largest earthquakes Mw 7.4, struck the western branch  
47 of the EARS in SW Tanzania (Rukwa area) on December, 1910 (Ambraseys, 1991) - though  
48 others consider it to have been Mw 7.3 (Midzi and Manzunzu, 2014). It did not cause large  
49 damage at that time because most of the houses were wooden made and were scattered owing to  
50 a small population at that time. Another earthquake in that order ( $M_s = 7.2$ ) occurred on 20<sup>th</sup>  
51 May, 1990 in Sudan, an areas considered to be the 350km extension of the EARS (Girdler and  
52 McConnell, 1994). The largest earthquakes within the Nyasa/Malawi rift (NMR) was in March  
53 1989 ( $M_w=6.1$ ) and December 2009 ( $M_w = 6.0$ ) in Salima and Karonga respectively (Jackson &  
54 Blenkinsop, 1997). While the NMR (Fig.1) is considered to be part of the western branch of the  
55 EARS it is in part associated with magmatism to its northern part, the Rungwe volcanic  
56 province. This northern part of the NMR is associated with magma / mantle plume below (e.g.  
57 Njinju et al, 2019). The central and southern parts are magma poor (e.g. Ebinger et al., 2019;  
58 Njinju et al., 2019). While the northern part of the NMR trends NNW-SSE, the central and  
59 southern parts of the NMR trend almost N-S with local variations. Kinematics of rifting of the  
60 NMR is debatable to-date (e.g. Delvaux, et al., 1992; Ebinger et al., 2019). Chorowicz (2005)  
61 for example considers the NMR to be like a part of southern segment of the 2,100km long  
62 western branch of the EARS. Further, Chorowicz (2005) considers the NMR to be part of the  
63 Tanganyika-Rukwa-Malawi fault zone that connects two main segments of the western branch.  
64 Using local earthquakes and source mechanisms from teleseismic earthquakes, Ebinger et al  
65 (2019) repute the NW-SE transform faulting by showing NE-SW (i.e.  $N58^\circ E$  and  $N65^\circ E$ )  
66 extension direction of the NMR. Similar works in support of the NE-SW extension of the

67 northern NMR are by Delvaux (1991), Delvaux et al. (1992), Morley (1999) and Macheyeke et al  
68 (2008). These controversies in the rifting kinematics of NMR is the main motivation for this  
69 research work.

70 **Fig. 1-**

71

72

### 73 **Regional structural geological setting**

74 The NMR is mostly underlain by Precambrian to Lower Palaeozoic Basement Complex rocks  
75 (Ray, 1975); and is located within the western branch of the EARS (Fig. 1). All the three mobile  
76 belts, Ubendian, Irumide and Mozambiquian affected the Basement Complex rocks across  
77 Malawi. Carter & Bennet (1973) identified that the three mobile belts occurred in two different  
78 tectono-metamorphic events. The first event involved the Ubendian Mobile belt from south  
79 western Tanzania, this event caused plastic deformation of the Basement Complex rocks and the  
80 second event involved both the Irumide and the Mozambiquian cycles; these two events were  
81 associated with brittle deformation of the Basement Complex rocks. Ubendian and  
82 Mozambiquian rocks dominate the Northern Province of Malawi whereas the Mozambiquian and  
83 Irumide mobile belts dominate the Southern province of the country (Carter & Bennet, 1973).

84 **Fig. 2-**

85 Carter & Bennet (1973) and Chapola (1997) describe tectonic structures of Malawi to be divided  
86 into two age groups namely; Pre-Cenozoic age structures and Cenozoic age structures.

87 The Pre-Cenozoic age structure mainly comprise those structures which were formed during the  
88 Karroo rifting of Permian to Triassic (~280 to 195 Ma) and Post Karroo rifting of Jurassic to

89 Cretaceous period (~195 to 65 Ma), these include faults, shear zones and dyke swarms. The  
90 Chimaliro fault zone which is to the southern side of the Champhira dome is an example of a  
91 Pre-Cenozoic structure. In southern Malawi NE-SW trending dyke swarms are examples of the  
92 Pre-Cenozoic structures.

93 The second group of structures comprises those structures which were formed during the  
94 Cenozoic age, these structures are associated with the initiation of the EARS, which in Malawi  
95 started about 10 million years ago. The general orientation of the rift related structures in both  
96 Northern and Southern Province of the NMR is mostly dominated by a NW-SE and N-S trending  
97 pattern with a minor NE-SW trending pattern. This, according to Delvaux, (1991) is a clear  
98 indication that the present orientation of the rift related structures is a reflection of the orogenic  
99 related structures orientation pattern most probably the Ubendian, Mozambiquian and Irumide  
100 mobile belts respectively. From this it can be deduced that the present orientation pattern of the  
101 rift related structures exist along the same orientation of the orogenic mobile belts (reactivated  
102 structures). Owing to its Z-like shaped, right-stepped pattern (Fig. 2), the NMR appears to be  
103 made of several rift segments.

#### 104 **Methodology**

105 Field work for this study was undertaken in October - November 2022 over a distance of 450km  
106 beginning in the central NMR southwards. The main objective for such an endeavor was to try to  
107 unveil the stress regime sequences and kinematics of the same. Focal mechanisms data from  
108 Ebinger et al (2019) were also modeled to obtain a present day stress field and kinematics. In the  
109 field, dip amount and dip direction of fault planes with or without slickensides were measured.  
110 Those without slickensides were considered as fracture planes or joints. For the planes with  
111 slickensides, the plunge amount and plunge directions of the same were also measured. Based on

112 whether or not fault planes or lines (slickensides) are relatively older or younger. The basis for  
113 grouping a fault plane (and the faulting event that caused the fault plane) as younger or older was  
114 purely based on field relationship considering presence or absence of minerals, type of minerals  
115 on a given plane, cross-cutting relationship between minerals and slickensides. Different  
116 slickensides which were encountered in the field were mainly Riedel shears, mineral steps and  
117 conjugate shear fractures. After these data and information were gathered, they were then entered  
118 in a Win-Tensor software developed by Damien Delvaux and processed using the procedures  
119 described in Delvaux and Sperner (2003).

120 Ten sites were visited namely ERM001 to ERM010 (Fig. 2). In this Chapter, eight localities are  
121 reported ERM002-8 and ERM010. ERM001 and ERM09 had fewer data to warrant presentation  
122 here. ERM02 and ERM003 are grouped together because they occur close to each other.  
123 Similarly, ERM004 and ERM005 are grouped together because of their proximity.

## 124 **Results**

125 *At Kasitu A and B, sites ERM002 and ERM003:* Both sites are within a few hundred meters and  
126 just on the western lake shore (Fig. 2, 3, 4) and about 120km by road south of Mzuzu town. They  
127 both portray 2 structural orientations; NNW-SSE, N-S and NNE-SSW. Large number of the  
128 structures are fresh high-angle faults (mainly conjugated joints or shear fractures), typically  
129 cross-cutting each other at  $\leq 60^\circ$ . Field relationship of these high-angle fracture planes indicate  
130 ENE-WSW opening of the rift.

131 **Fig. 3 –**

132 **Fig. 4 –**

133 In general, the fault slip data in both sites indicate three sets of fault planes; (a) sub-vertical  
134 planes with dip amounts between 75° and 88°: these have sub-horizontal slip-lines <20°, typically  
135 6° to 19°. These slip-lines indicate both sinistral and dextral shear movements-they are  
136 interpreted as strike-slip fault planes; (b) planes dipping between 54° and 68°: Most of these  
137 fault planes are conjugated and oriented NW-SE. They are interpreted as normal fault planes  
138 indicating rift opening in an ENE-WSW; and (c) shallow – angle dipping planes (approximately  
139 40°): These fault planes are oriented NE-SW. Direction of movement in one of the slip lines on  
140 these fault planes is NE-SW (i.e. 39° towards 028°). These types of faults are showing oblique  
141 opening along NE-SW, sub-parallel to the orientation of the fault planes themselves.

142 It can be summarized therefore that opening of the rift at both Kasitu A and B is ENE-WSW and  
143 NE-SW regardless of the type of structures in which the movement is occurring. Modelled stress  
144 tensor for these sites indicate normal faulting regime with radial extension stress regime with  
145  $S_{hmin}=151^\circ$ ,  $S_{Hmax} = 061^\circ$  (Fig. 3, Table 1).

146 **Table 1 –**

147 *At Diwangu and Bua rivers, sites ERM004 and ERM005* (Fig. 5): These points are located 60m  
148 from Kasitu sites along the lake shore. Unlike ERM002 and ERM003 at Kasitu, ERM004 and  
149 ERM005 are characterized by two fault trends; NW-SE and NNW-SSE. The main fault planes  
150 are high-angle faults, typical of strike-slip faults and are oriented in such a way that those faults  
151 that dip to the east and trending NW-SE are characterized by sinistral sense of movement  
152 whereas those that dip to the southwestern side are characterized by dextral sense of movement  
153 (Fig. 6). Foliation fabric of the Precambrian basement measured here dip 40° towards 220°.

154 **Fig. 5 –**

155

**Fig. 6-**

156 *At Kazipur river bridge: site ERM006:* This site is located on the southern part of the NMR  
157 (Fig. 2, 3, 6). It is characterized by NW-SE trending faults which are the major ones here. NE-  
158 SW trending faults are also present but comparably less pronounced than the former. There are  
159 also W-E trending faults. While all the three sets of faults seem to be relatively younger (i.e.  
160 Cenozoic), the W-E trending faults seem to be the youngest owing to their fresher surfaces and  
161 echelon pattern in most places, typical of isolated fault strands. The E-W faults are less  
162 penetrative, probably restricted to upper crust tectonics.

163 In the same site are E-W trending thrust faults. The planes of movement are associated with  
164 quartz-hornblende minerals implying that they are the oldest faults in the area. A pervasive brittle  
165 deformation in the area is exemplified by fault breccia, most likely related to Karoo rifting. The  
166 thrust faults are also attributed the Karoo tectonics. In the same area are tight folds, characterized  
167 by NNW-SSE trending axial plane. These ductile-semi ductile deformation structures seem to  
168 have been formed by NNE-SSW compressive stress field. In summary, the tectonic events in the  
169 area are as follows: (a) metamorphism of the Precambrian basement, (b) folding of the basement,  
170 (c) thrusting associated with quartz-hornblende mineralization, (d) faulting associated with  
171 breccia, (e) recent deformation associated with the barren faults (strike slip and normal faults)-of  
172 all these the E-W faults are the youngest (Fig. 8a, b). The overall stress field from modelled  
173 stress tensor corresponding to the present stress kinematics is shown in Figure 3. It is  
174 characterized by an oblique transtensive stress field oriented NNE-SSW with  $S_{Hmin}=020^\circ$ ,  
175  $S_{Hmax}=110^\circ$ .

176

**Fig. 7 –**

177

**Fig. 8a –**

178

**Fig. 8b-**

179 About 10km south of Kazipuru river is the Mua site, ERM007 (Fig. 2, 3, 9). This is a place  
180 where a fresh cut of a fault scarp is observed. Water falls on the scarp in such a way that one can  
181 visualize the recent faulting. Most of the faults here are high-angle faults meaning that the  
182 normal fault related scarp was formed from reactivation of strike-slip faults. Few measurements  
183 taken at this point indicate that the fault planes dip between  $68^{\circ}$  and  $74^{\circ}$  and the slip lines show  
184 block movements at  $40^{\circ}$  dip amount towards NW ( $336^{\circ}$ ).

185 Nearly 80km SE of this site is the Malombe site. It is located just east of the Malombe fault and  
186 west of Lake Malombe. Like for most fault planes in this area, the fault planes here are mostly  
187 high-angle faults  $70^{\circ}$  to sub-vertical, generally dipping to the north and NNE. The prominent  
188 structures at Malombe site are the NNW-SSE that dip due north to NNE. Slip vectors along the  
189 fault planes vary from N to E, meaning that there are faults that open in a N-S direction and those  
190 that open in an E-W direction. The latter are less prominent whereas the faults that open in a N-S  
191 direction are prominent and are more deep seated than at Kazipuru site (ERM006).

192 On the western site of Malombe site where the Malombe fault is located, landslide is clear. This  
193 landslide has affected most of the rocks units and has equally disturbed the orientation of the  
194 structures on the hanging wall side including the structures at the Malombe site (ERM008).

195

**Fig. 9 –**

196 *At Twabwa Quarry: site ERM010:* This site is more than 200km by road south of ERM008. It is  
197 along the NW-SE trending Chyolo active fault (Fig. 2, 3,10).

198 Both dip slip and lateral movements characterize this fault and both components seem to occur  
199 together in any given plane. The prominent sense of movement in all the faults in this southern

200 most part of the rift is sinistral. Three types of faults are recognized from their planes and slip  
201 movements; normal faults, strike-slip and thrust faults. The latter is quartz veined and therefore  
202 older than the normal and strike slip faults (the barren ones). The oldest tectonic structures in the  
203 area are the S-C fabrics associated with Precambrian deformational events. The modelled stress  
204 tensor corresponding to the most recent rifting stress field is presented in Figure 3. It indicates  
205 that this southernmost part of the NMR is opening obliquely along the N-S direction. Comparing  
206 site ERM006, ERM008 and ERM010 in terms of level of N-S opening slickensides, it is evident  
207 that the magnitude is increasing southerly. The slickensides and the fault planes in which they  
208 occur are clearer as one moves from central part of the NMR to the southern part (i.e. from  
209 ERM006 to ERM010, Fig. 11).

210 **Fig. 10 –**

211 **Fig. 11-**

## 212 **Discussion**

213 According to Daly (1998), the NW-SE trending Precambrian Ubendian structures are ductile to  
214 semi-ductile shear zones and folds. These are intersected by NE-SW trending Karoo shear zones  
215 and faults (Normal and strike-slip faults such as the Ruhuhu, Ruangwa and Maniamba troughs  
216 (e.g. Njinju et al. 2019). The zones of intersections were, and are still the weakest structural  
217 zones in the entire rift subject of future fault reactivation and locus of deep seated magmatism.

218 Delvaux et al (1992) and Njinju et al (2019) show that the Cenozoic rifting reactivated  
219 Precambrian structures (shear zones). According to Delvaux et al. (1992), the reactivation in Late  
220 Miocene to Pleistocene was a near radial extensive regime and was followed by strike-slip  
221 faulting (compressive regime) in the Late Pleistocene. Both the Late Miocene-Pleistocene and

222 the Late Pleistocene tectonic events were associated with the magmatic pulses in the Rungwe  
223 volcanic province.

224 This work has demonstrated five major findings from fault slip data collected from the central  
225 part to the southern part of the NMR:

226 First of all; the central part is under radial extension. This is compatible with the Late Miocene-  
227 Pleistocene rifting model reported by Delvaux et al (1992) for the northern part of the NMR.  
228 Such results indicate that the radial extension is from the central part to the northern part of the  
229 rift. Radial extension means opening of the rift in all directions- a phenomenon that is attributed  
230 to plume activities or lithospheric scale magmatic activities (e.g. Reiss et al., 2021). Second; the  
231 southern half of the NMR is under oblique NNE-SSW transtensive tectonic regime with  $Sh_{min} =$   
232  $020^{\circ}$ . Third; further south, the obliquity extension rotates by about  $15^{\circ}$  reaching N-S direction  
233 with  $Sh_{min} = 175^{\circ}$  (Table 1, Fig. 3). Type localities for this N-S extension phenomena were  
234 recorded in Kazipuru river (ERM006), Malombe fault (west of Lake Malombe, ERM008) and  
235 Twabwa area along the Thyolo fault (ERM010). Forth; the level of structural penetration and  
236 intensity of faulting show that the N-S opening is more pronounced in the south than towards the  
237 north, and fifth; the faults that dip to the east and trending NW-SE are characterized by sinistral  
238 sense of movement whereas those that dip to the southwestern side are characterized by dextral  
239 sense of movements. It implies that the rift is essentially under normal faulting regime but with a  
240 significant strike –slip component – hence the obliquity kinematics.

241 As most of the data collected on the Malawi side indicate that fault planes dipping to the east  
242 have sinistral sense of movement as contrasted by the fault planes dipping to the western side  
243 which have dextral sense of movement, it implies that most of the faults in Malawi (i.e. middle

244 and southern part) are under sinistral oblique faults and the faults in the northern segment that  
245 dips to the west are under dextral sense of movements.

246 Modeled stress tensors from focal mechanism data compiled by Ebinger et al. (2019) for small to  
247 moderate earthquakes that occurred in the last half a century (1968 to 2019) consistently indicate  
248 a pure extension regime oriented NNW-SSE ( $\text{Shmin} = 165$ ), implying normal faulting events  
249 only. However, looking at individual seismic data for the area, strike-slip events are present, and  
250 though are few, they are generally related to over 30km deep events meaning that they are  
251 related to the lithospheric segments. As most of the reported seismic events in the area for the  
252 last 50 years are small to moderate, it appears that they are related to shallow seated events, most  
253 likely upper crust faulting events. It should be noted that, small to moderate earthquakes whether  
254 magmatic or tectonic in origin or both, are generally not able to leave a mark on the rocks  
255 (McCalpin, 1996; Keller and Pinter 2002). In other words, earthquakes larger than moderate  
256 earthquakes are the ones that can leave marks (slickenlines) on rocks and that fault slip data are  
257 the ones related to large earthquakes. It has to be made clear here that even the upper crustal  
258 tectonic activities can cause large earthquakes and small earthquakes may come from middle to  
259 lower crust (Yang and Chen, 2010).

260 Putting both fault slip and focal mechanism data into regional perspective, it can be implied that,  
261 the NMR has not been deforming in the same way both in time and space. During the Late  
262 Pleistocene, the lithospheric scale deformation assisted by mantle plume, affected the middle to  
263 northern part of the rift which is magma rich causing it to open radially. This explains why the  
264 middle / central part of the NMR are under radial extension. Delvaux et al (1992) also report  
265 radial extension related to Miocene – Pleistocene. It means that this event continued to Late  
266 Pleistocene or even to Holocene and is still ongoing or was repeated some thousand years before

267 present (episodic rifting). During the same time (Late Pleistocene to Holocene), the southern part  
268 was opening obliquely under the so called oblique NNE-SSW transtensive regime and further to  
269 the southern end, it was opening in an oblique N-S extensive regime.

270 It is though difficult to comprehend a N-S extension within a generally N-S oriented NMR.  
271 Owing to freshness of the N-S opening structures (Fig. 8) and the relatively less penetrative field  
272 relationship, it can be implied that these structures are related to upper crust deformation  
273 activities which are related to secondary faults (e.g. Maerten et al., 2002) developed by local  
274 stress perturbations (e.g. Maerten et al., 2002; Chen et al., 2008; Feng et al., 2020) in the process  
275 of rifting caused by active / and far field stresses. Stress perturbations, and hence changes of  
276 positions of the principal stress axis  $\sigma_1$  can occur as a result of pre- and post- seismic stress states  
277 differences (e.g. Hasegawa et al., 2012; Yoshida et al., 2014; Feng et al., 2020) and pore pressure  
278 changes (e.g. An et al., 2021). As the NMR is still a younger rift and more particularly towards  
279 its southern tip, it is not surprising to find these intra basinal sub-orthogonal structures to the rift  
280 being developed (e.g. Fig. 8a, b) and are more important towards the southern (relatively  
281 youngest) tip of the rift (Fig. 11).

282

## 283 **Conclusion**

284 The northern to middle part of the NMR is under radial to sub-radial extension because of both  
285 tectonic and possibly magma activities. The southern part of the rift is opening obliquely in the  
286 NNE-SSW to N-S. The latter kinematics is considered to be attributed to stress perturbations at  
287 the upper crustal level, the process that is actively ongoing in the NMR. Therefore, the actual  
288 active regional opening direction of the NMR to its southern part, hereby reported is NNE-SSW  
289 characterized by an oblique transtensive stress field with  $Sh_{min} = 020^\circ$  and  $R' = 1.91$  meaning

290 that faulting / rifting has both normal and strike-slip components. This NNE-SSW extensional  
291 direction for the NMR obtained from this work is somewhat in disagreement with some of the  
292 published extensional directions that attests to NE-SW directions (e.g. Ebinger et al, 2019,  
293 extension direction N58°E and N65°E) and NW-SE (e.g. Ring and Betzler; 1995; Chorowicz,  
294 2005).

295

296

297

298

## 299 **References**

300 Ambraseys, N.N. (1991). The Rukwa earthquake of 13 December 1910 in East Africa. *Terra*  
301 *Nova*, 3(2), 202–211. doi:10.1111/j.1365-3121.1991.tb00873.x

302 An, M., Zhang, F., Dontsov, E., Elsworth, D., Zhu, H. & Zhao, L. (2021). Stress perturbation  
303 caused by multistage hydraulic fracturing: Implications for deep fault reactivation.  
304 *International Journal of Rock Mechanics and Mining Sciences*, 141,  
305 104704. doi:10.1016/j.ijrmms.2021.104704

306 Bott, M.H.P. (1995). Mechanisms of rifting: geodynamic modeling of continental rift systems.  
307 *In: Olsen, K.H. (Ed.), Continental Rifts: Evolution, Structure, Tectonics. Elsevier Series:*  
308 *Amsterdam*, 409-436p.

- 309 Bott, M.H.P. (2006). Mechanisms of rifting: Geodynamic modeling of continental rift systems.  
310        Developments in Geotectonics, 27–43. doi:10.1016/s0419-0254(06)80006-6
- 311 Buck, W.R. (1991). Modes of continental lithospheric extension. Journal of Geophysical  
312        Research, B, Solid Earth and Planets 96(12), 20161–20178.
- 313 Carter, G.S. & Bennet, J.D. (1973). The Geology and Mineral Resources of Malawi.
- 314 Chapola, L. (1997). State of stress in East and Southern Africa and Seismic Hazard Analysis of  
315        Malawi [Institute of Solid Earth Physics, University of Bergen, Norway (MSc Thesis).].  
316        [http://www.researchgate.net/post/How\\_do\\_I\\_extract\\_lineaments\\_from\\_Landsat\\_Image\\_and](http://www.researchgate.net/post/How_do_I_extract_lineaments_from_Landsat_Image_and_RADAR)  
317        [RADAR](http://www.researchgate.net/post/How_do_I_extract_lineaments_from_Landsat_Image_and_RADAR)
- 318 Chen, Y.Z., Lin, X.Y. & Wang, Z.X. (2008). T-stress evaluation for slightly curved crack using  
319        perturbation method. International Journal of Solids and Structures 45, 211–224
- 320 Chorowicz, J. (2005). The East African rift system. J. Afr. Earth Sci. 43, 379-410
- 321 Corti, G., Bonini, M., Conticelli, S., Innocenti, F., Manetti, P. & Sokoutis, D. (2003). Analogue  
322        modelling of continental extension: A review focused on the relations between the  
323        patterns of deformation and the presence of magma, Earth Sci. Rev., 63, 169 – 247.  
324        [https://doi.org/10.1016/S0012-8252\(03\)00035-7](https://doi.org/10.1016/S0012-8252(03)00035-7)
- 325 Delvaux, D. (1991). The Karoo to recent rifting in the western branch of the East-African Rift  
326        System: a bibliographical synthesis. Musee Roy. Afr. Central Tervuren (Dép. Géol. Min.,  
327        Rap. Ann.) 1989–1990, 63–83.
- 328 Delvaux, D. & Sperner, B. (2003). Stress tensor inversion from fault kinematic indicators and  
329        focal mechanism data: the TENSOR program. *In*: Nieuwland, D. (Ed.), New Insights into

330 Structural Interpretation and Modelling, vol. 212. Geological Society of London, Special  
331 Publication, pp. 75–100.

332 Delvaux, D. & Barth, A. (2010). African stress pattern from formal inversion of focal  
333 mechanism data. Implications for rifting dynamics. *Tectonophysics* 482, 105– 128.

334 Delvaux, D., Levi, K., Kajara, K. & Sarota, S. (1992). Cenozoic Paleostress and Kinematic  
335 Evolution of the Rukwa - North Malawi Rift Valley (East African Rift System). *Bulletin*  
336 *du Centre de Recherches elf Exploration Production elf Aquitaine* (16/2), 383–406.

337 Win-tensor software by Damien Delvaux of 5<sup>th</sup> October, 2021. (Version 5-9-2) [Dataset].  
338 [https://www.damiendelvaux.be/Tensor/WinTensor/win-tensor\\_download.html](https://www.damiendelvaux.be/Tensor/WinTensor/win-tensor_download.html)

339 Feng, C., Yang, Y., Ma, X., Qi, B., Zhang, P., Meng, J., Tan, C. & Chen, Q. (2020). Local stress  
340 perturbations associated with the 2008 Wenchuan M 8.0 earthquake near the  
341 Longmenshan fault zone in the eastern margin of the Tibetan Plateau. *Journal of Asian*  
342 *Earth Sciences*, 200, 104429. doi:10.1016/j.jseas.2020.104429

343 Girdler, R. W. & McConnell, D.A. (1994). The 1990 to 1991 Sudan Earthquake Sequence and  
344 the Extent of the East African Rift System. *Science*, 264(5155), 67–  
345 70. doi:10.1126/science.264.5155.67

346 Gueydan, F. & Précigout, J., 2014. Modes of continental rifting as a function of ductile strain  
347 localization in the lithospheric mantle. *Tectonophysics*, 612-613, 18–  
348 25. doi:10.1016/j.tecto.2013.11.029

349 Hasegawa, A., Yoshida, K., Asano, Y., Okada, T., Linuma, T. & Ito, Y., 2012. Change in stress  
350 field after the 2011 great Tohoku-Oki earthquake. *Earth Planet. Sci. Lett.* 355–356, 231–  
351 243.

352 Hao, L., Loon, A.J.V., Xu, J., Tian, L. & Chen, D. (2020). Relationships between tectonic  
353 activity and sedimentary source-to-sink system parameters in a lacustrine rift basin: a  
354 quantitative case study of the Huanghekou Depression (Bohai Bay Basin, East China).  
355 Basin Res. 32, 587–612.

356 Jackson, J. & Blenkinsop, T. (1997). The Bilila-Mtakataka fault in Malaŵi: An active, 100-km  
357 long, normal fault segment in thick seismogenic crust. *Tectonics*, 16(1), 137–150.  
358 <https://doi.org/10.1029/96TC02494>

359 Keller, A. & Pinter, N. (2002). *Active tectonics. Earthquakes, Uplift and Landscape*. 2d ed.  
360 Prentice Hall Earth Sciences Series: New Jersey, 362pp.

361 Macheyeke, A.S., Mdala, H., Chapola, L.S., Manhiça, V.J., Chisambi, J., Feitio, P., Ayele, A.,  
362 Barongo, J., Ferdinand, R. W., Ogubazghi, G., Goitom, B., Hlatywayo, J. D., Kianji, G. K.,  
363 Marobhe, I., Mulowezi, A., Mutamina, D., Mwano, J. M., Shumba, B. & Tumwikirize, I.  
364 (2015). Active fault mapping in Karonga-Malawi after the December 19, 2009 Ms 6.2  
365 seismic event. *Journal of African Earth Sciences*, 102, 233–246.  
366 <https://doi.org/10.1016/j.jafrearsci.2014.10.010>

367 Macheyeke, A.S., Delvaux, D., De Batist, M. & Mruma, A. (2008). Fault kinematics and tectonic  
368 stress in the seismically active Manyara-Dodoma rift branch in Central Tanzania –  
369 Implications for the East African Rift. *J. Afr. Earth Sci.* 51, 163–188.

370 Maerten, L., Gillespie, P. & Pollard, D.D. (2002). Effects of local stress perturbation on  
371 secondary fault development. *Journal of Structural Geology* 24, 145-153.

372 McCalpin, J.P. (Ed.) (1996). *Paleoseismology*. Academic Press: New York, 583pp.

373 Midzi, V. & Manzunzu, B. (2014). 15 - Large recorded earthquakes in sub-Saharan Africa. Part  
374 IV - Case studies: Africa. Cambridge University Press:

375 Prodehl, C., Fuchs, K. & Mechie, J. (1997). In: Structure and dynamic processes in the  
376 lithosphere of the Afro-Arabian rift system. Ed.: K. Fuchs. Amsterdam 1997. S. 1-13.  
377 (Tectonophysics. 278,1/4.)

378 Ray, G.E. (1975). The Geology of the Chitipa - Karonga Area.  
379 <http://www.bgs.ac.uk/research/highlights/2010/malawiMineralPotential.html>

380 Reiss, M.C., Muirhead, J.D., Laizer, A.S., Link, F., Kazimoto, E.O., Ebinger, C.J. & Rumpker,  
381 G. (2021). The impact of complex volcanic plumbing on the nature of seismicity in the  
382 developing magmatic Natron rift, Tanzania Miriam Christina. *Front. Earth Sci.*, 23 Sec.  
383 *Volcanology*. <https://doi.org/10.3389/feart.2020.609805>

384 Ring, U. & Betzler, C. (1995). Geology of the Malawi Rift: kinematic and tectonosedimentary  
385 background to the Chiwondo Beds, northern Malawi. *Journal of Human Evolution*, 28(1),  
386 7–21. doi:10.1006/jhev.1995.1003

387 Shillington, D. (2010). Continental Breakup in East Africa – State of the Planet.  
388 <http://blogs.ei.columbia.edu/2010/02/05/continental-breakup-in-east-africa/>

389 Yang, Z., & Chen, W.-P. (2010). Earthquakes along the East African Rift System: A multiscale,  
390 system-wide perspective, *J. Geophys. Res.*, 115, B12309, doi:10.1029/2009JB006779

391 Yoshida, K., Hasegawa, A., Okada, T. & Linuma, T. (2014). Changes in the stress field after the  
392 2008 M 7.2 Iwate-Miyagi Nairiku earthquake. *J. Geophys. Res. Solid Earth* 119, 9016–  
393 9030.

394

395 **List of Figures**

396 Fig. 1- (B) Schematic diagram of the East African Rift System showing approximate location of the study area  
397 indicated by the red rectangle (Fig. 2). Insert A is a satellite map of the East African Rift System (Shillington, 2010),  
398 showing location of map B. NMR = Nyasa / Malawi rift. Modified from Macheyeke et al. (2015).

399 Fig. 2- Visited sites in the study area (See Fig. 1 for location)

400 Fig. 3 –Modelled stress field from fault slip-data (paleostress analysis) to the right against modelled focal  
401 mechanisms data (to the left) plotted on google earth snapshot. The focal mechanisms data are for the  
402 southern and northern part of the NMR whereas the fault slip data are for the middle and southern part of  
403 the NMR. Focal mechanism data are from Ebinger et al (2019). For coordinates of sites visited see Figures  
404 2, 4-5, 7,9-10. Compare with Table 1

405 Fig. 4 – The high resolution DEM of Kasitu A, and Kasitu B sites

406 Fig. 5 – The high resolution DEM of Diwangu and Bua river sites

407 Fig. 6- Model of sense of movement for fault planes at Diwangu and Bua rivers

408 Fig. 7 – The high resolution DEM of Kazipuru river bridge site

409 Fig. 8a – E-W trending echelon joints at Kazipuru river bridge

410 Fig. 8b- Conceptualized model of the E-W echelon joints / fractures at Kazipuru river bridge

411 Fig. 9 – The high resolution DEM of Malombe site

412 Fig. 10 – The high resolution DEM of Twabwa Chyolo site

413 Fig. 11- The oblique normal faults opening N-S at Thyolo site. Their displacements are larger than those in sites  
414 ERM006 and ERM008, over 200km north of this site. Upper panel is without annotation and the lower panel is with  
415 annotated fault plane (s)

416

417 **Table 1:** – Stress tensor parameters obtained from fault slip data and focal mechanisms for the NMR. (n): number  
418 of data used in the inversion, (nt): total number of data in the database, ( $\sigma_1$ ,  $\sigma_2$  and  $\sigma_3$ ) are the principal

419 stress axes, i.e. maximum, intermediate and minimum respectively, (R): stress ratio, (QRw): quality rank,  
420 (R'): stress regime index, (Reg): stress regime according to the World Stress Map, (SHmax, Shmin):  
421 respectively, maximum and minimum horizontal principal stress directions. ( $\sigma$  mag): normal stress  
422 magnitude, ( $\tau$  mag): shear stress magnitude and ( $\Theta$ ) the angle between normal and shear stress

423

## 424 **Acknowledgements**

425 This mission was made possible through the warm collaboration between the Geological Survey  
426 Department of Malawi (MGSD). We particularly thank Mr. Kondwani Dombola, the Acting  
427 Director of the MGSD for accepting the request of the first author to work with the Survey. The  
428 MGSD made available to the researchers, the resources such as data, field vehicle and organized  
429 for field logistics throughout the time we were in Malawi. We are indebted to Mr. Patrick  
430 Chindandali and Mr Yohane Kaukutu (Librarian) both from MGSD for making available to us  
431 some literatures useful for our work. Special thanks to Rebeka B. Mwakalinga from Tanzania for  
432 joining us in the field. Mr Benjamin Chirwa provided a safe and warm driving throughout the  
433 fieldwork. We also thank each and every one who in one way or another supported us.

# **Paleostress analysis of the Nyasa / Malawi Rift: implication for the present-day regional dynamics**

Athanas S. Macheyeke<sup>(1,2)</sup> and Hassan Mdala<sup>(3)</sup>

<sup>(1)</sup> Department of Geology, College of Earth Sciences and Engineering, the University of Dodoma-Tanzania

[asmacheyeke@yahoo.com](mailto:asmacheyeke@yahoo.com)

<sup>(2)</sup> Earth Sciences Institute of Shinyanga, P. O. Box 1016, Shinyanga-Tanzania

<sup>(3)</sup> Geological Survey Department of Malawi, Regional Office North, Pvt Bag 9, Mzuzu, Malawi

Table 1 –

Site ID	Location	n	nt	$\sigma_1$	$\sigma_2$	$\sigma_3$	R	R'	SHmax	Shmin	Regime	Stress Regime	$\Theta$	$\sigma$ mag	$\tau$ mag	QRw
ERM002/3	Kasitu A/B	6	12	80/168	02/064	10/333	0.2	0.2	61	151	NF	Radial EXTENSIVE	24.8	30.4	16	D
ERM006	Kazipuru river	11	11	39/108	41/333	25/220	0.09	1.91	110	20	NS	Oblique TRANSTENSIVE	38.5	37.7	31.7	C
ERM010	Thabwa- (Thyolo Fault)	6	7	50/250	35/104	17/001	0.54	0.54	85	175	NS	Oblique EXTENSIVE	35.7	42.5	26.8	D
Focal Mechanisms- All data		11 2	18 8	88/176	00/075	02/345	0.36	0.36	75	165	NF	Pure EXTENSIVE	35.7	54.7	36.6	A
Focal mechanisms – Northern		62	12 6	82/135	03/246	08/336	0.41	0.41	73	163	NF	Pure EXTENSIVE	34.7	53.4	34.4	A
Focal mechanisms – Southern	FM data	71	80	80/069	10/253	01/163	0.28	0.28	67	157	NF	Pure EXTENSIVE	37.8	55	40.2	A

Figure 1.

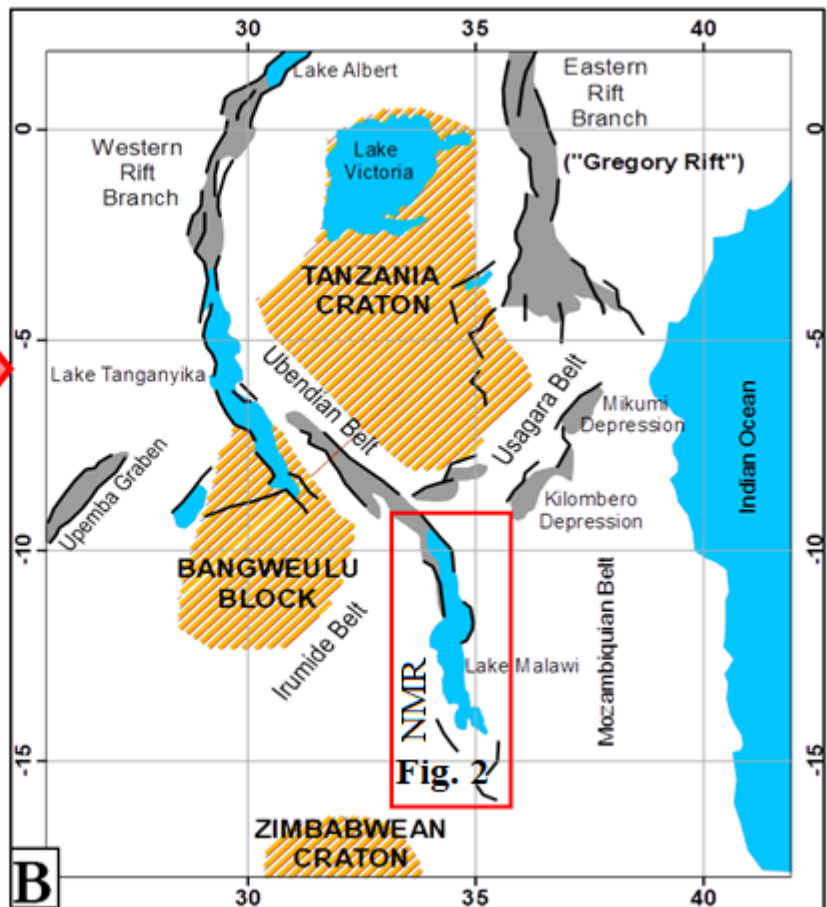
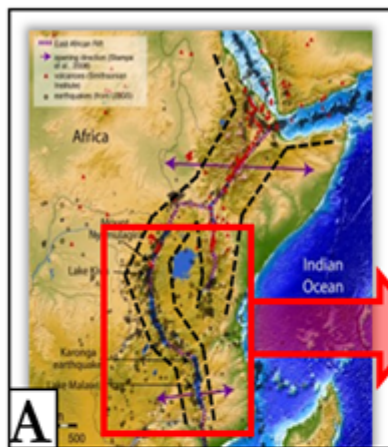


Figure 2.

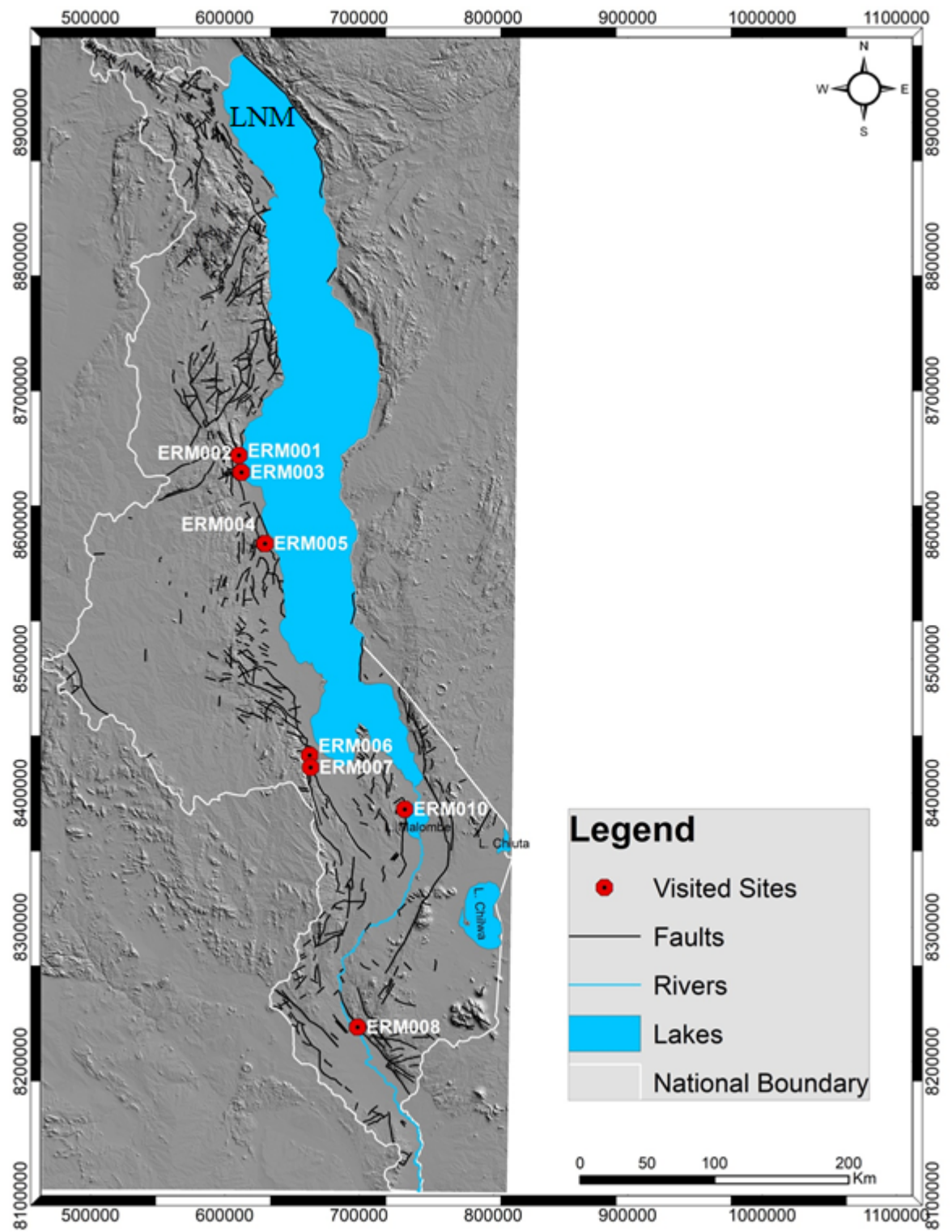
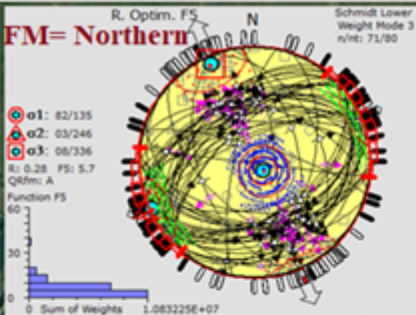
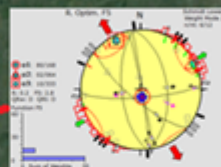


Figure 3.

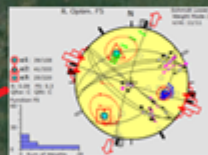


EMR002  
EMR001  
EMR004  
EMR005

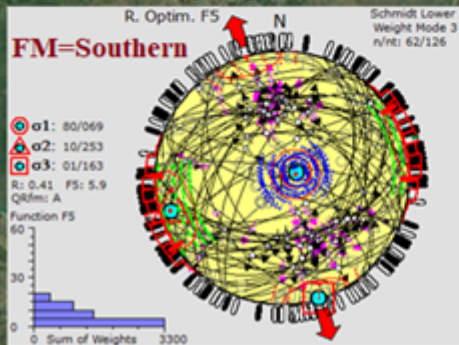


Radial Extensive  
All directions

ERM06  
ERM07  
ERM08



Oblique  
transverse  
NNE-SSW



ERM09



Oblique  
Extensive  
N-S

ERM010

Figure 6.

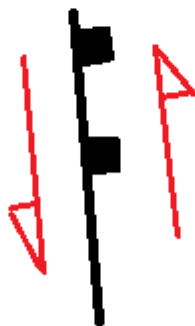
**Northern rift  
(segment)**



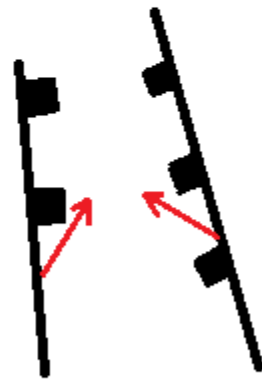
**Dextral sense of movement on westerly dipping faults / fault planes (both dip and lateral movements occur)**



**Southern rift  
(segment)**



**Sinistral sense of movement on easterly dipping faults / fault planes (both dip and lateral movements occur)**



**Effective transport  
of materials**

Figure 8b.

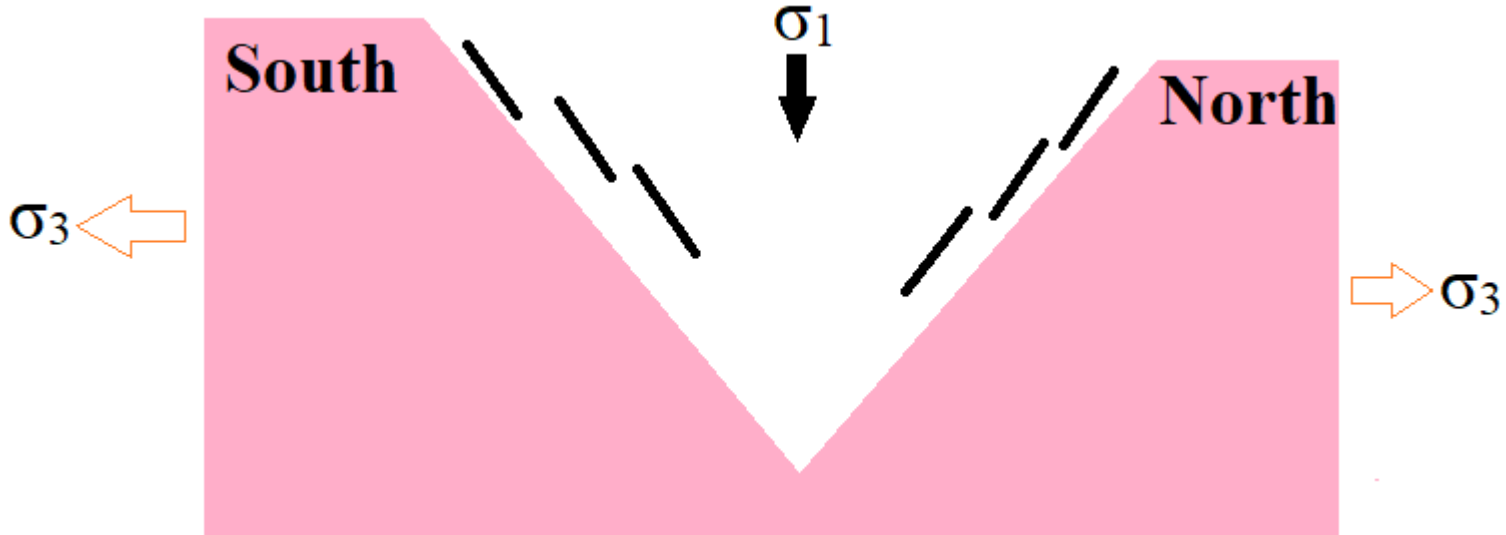


Figure 8a.



Man in field vest and glasses, holding a clipboard, standing on the rocks.

Man in field vest sitting on a rock, holding a yellow book.

Downward-pointing arrows overlaid on the rocky terrain.

Person in a blue cap and red shirt washing items in a green tub near the water.

Red bag or equipment lying on the ground in the foreground.

Figure 11.

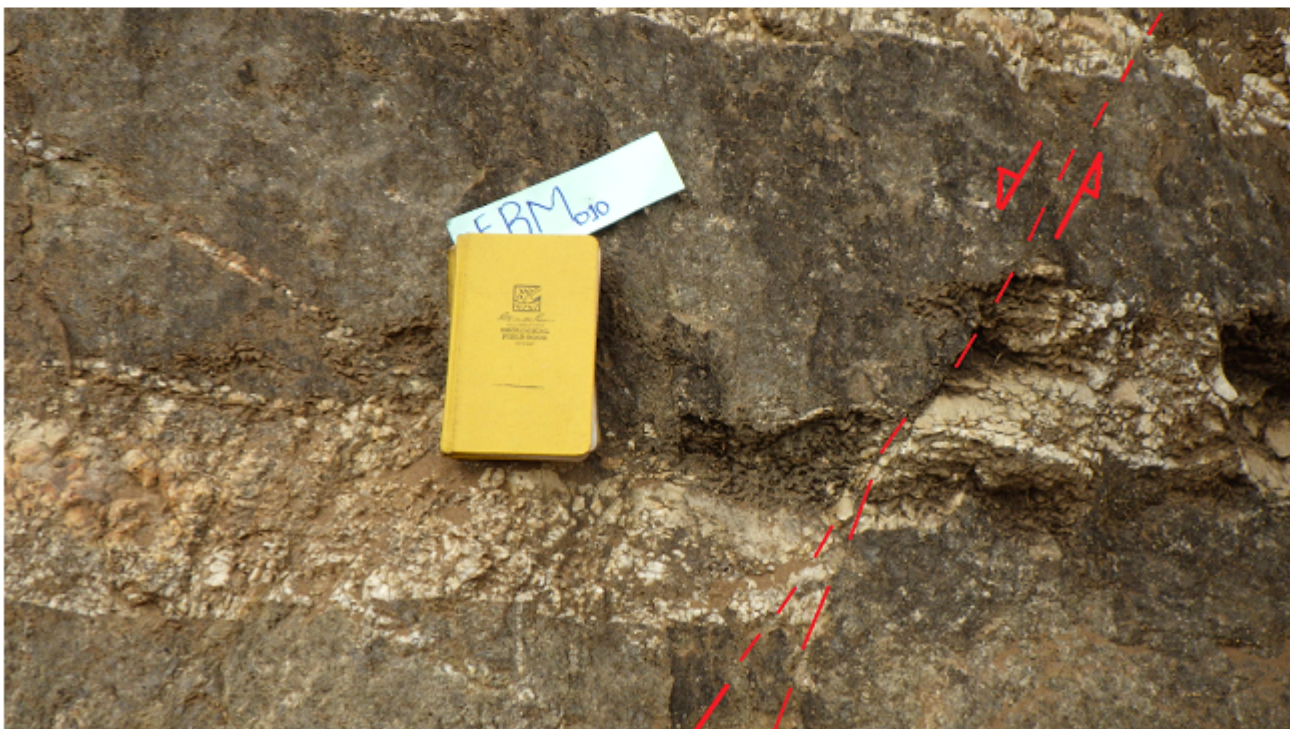


Figure 4.

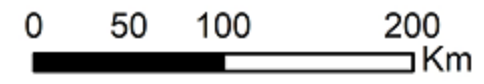
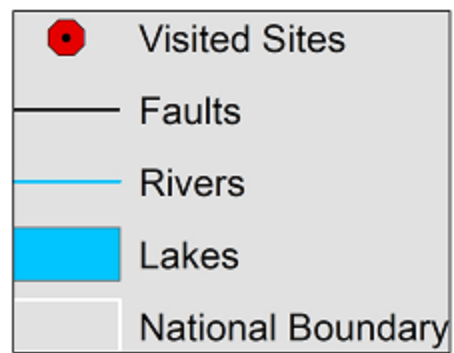
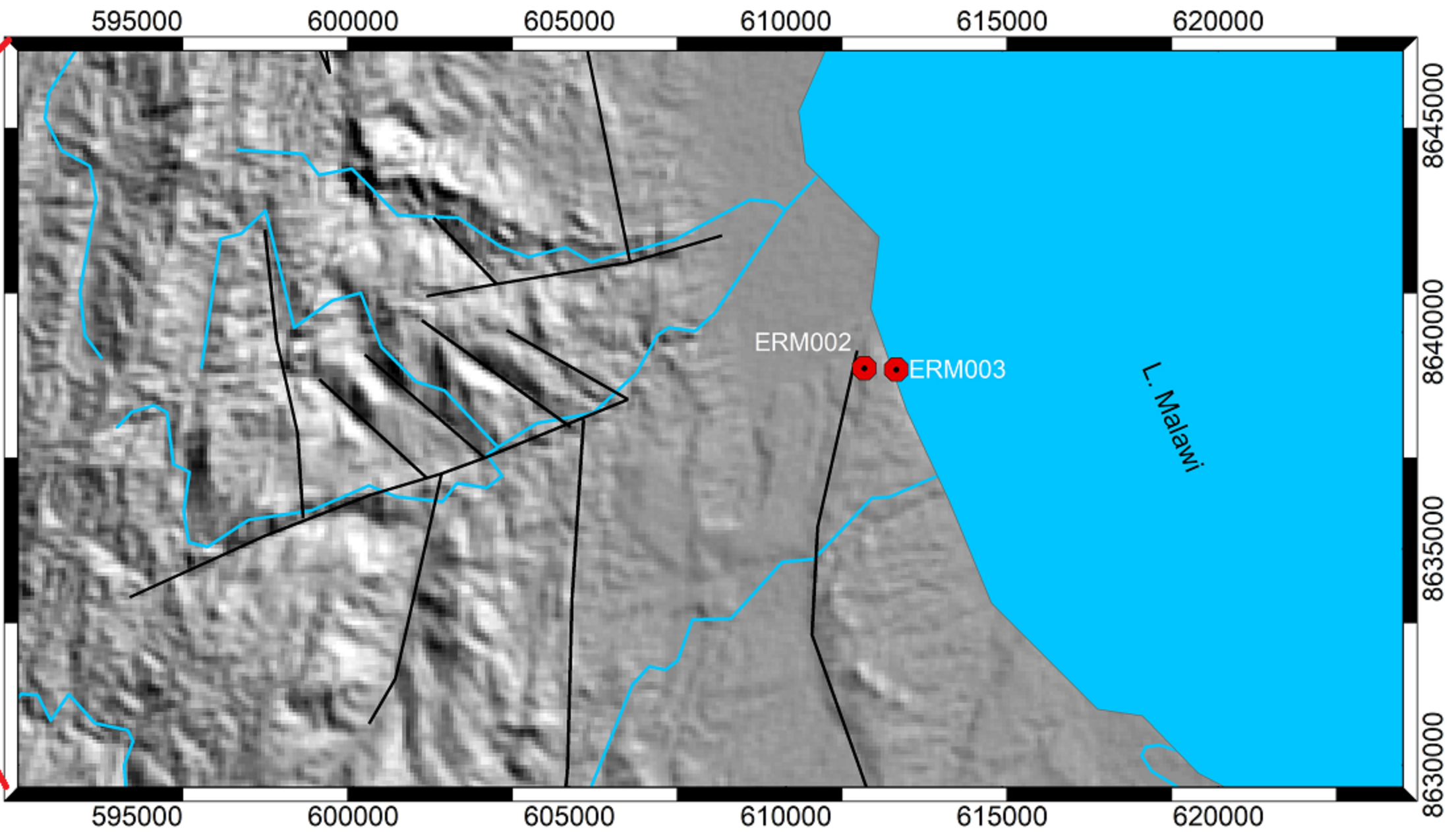
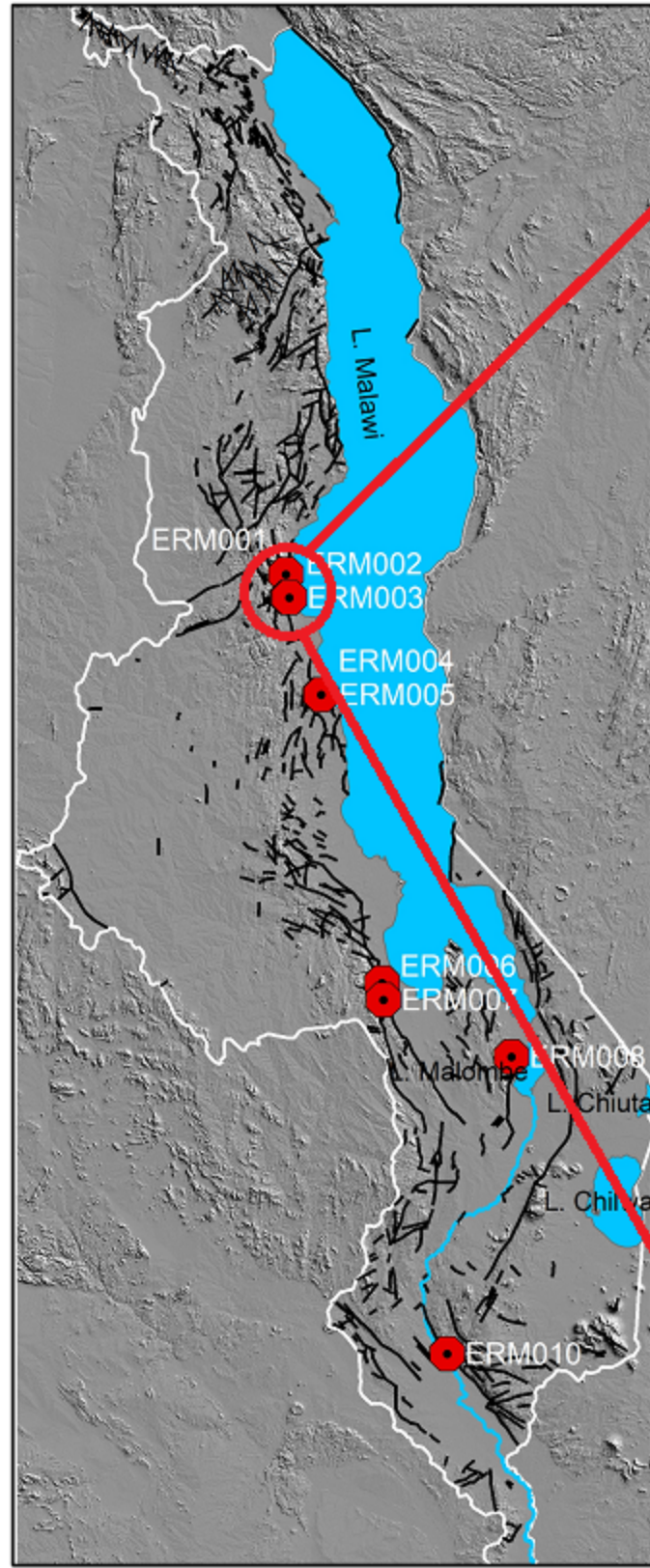


Figure 7.

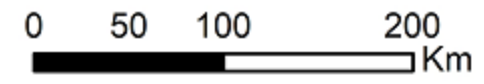
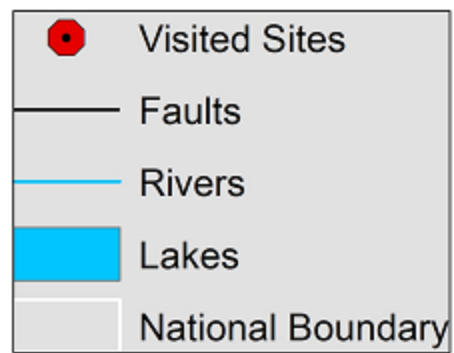
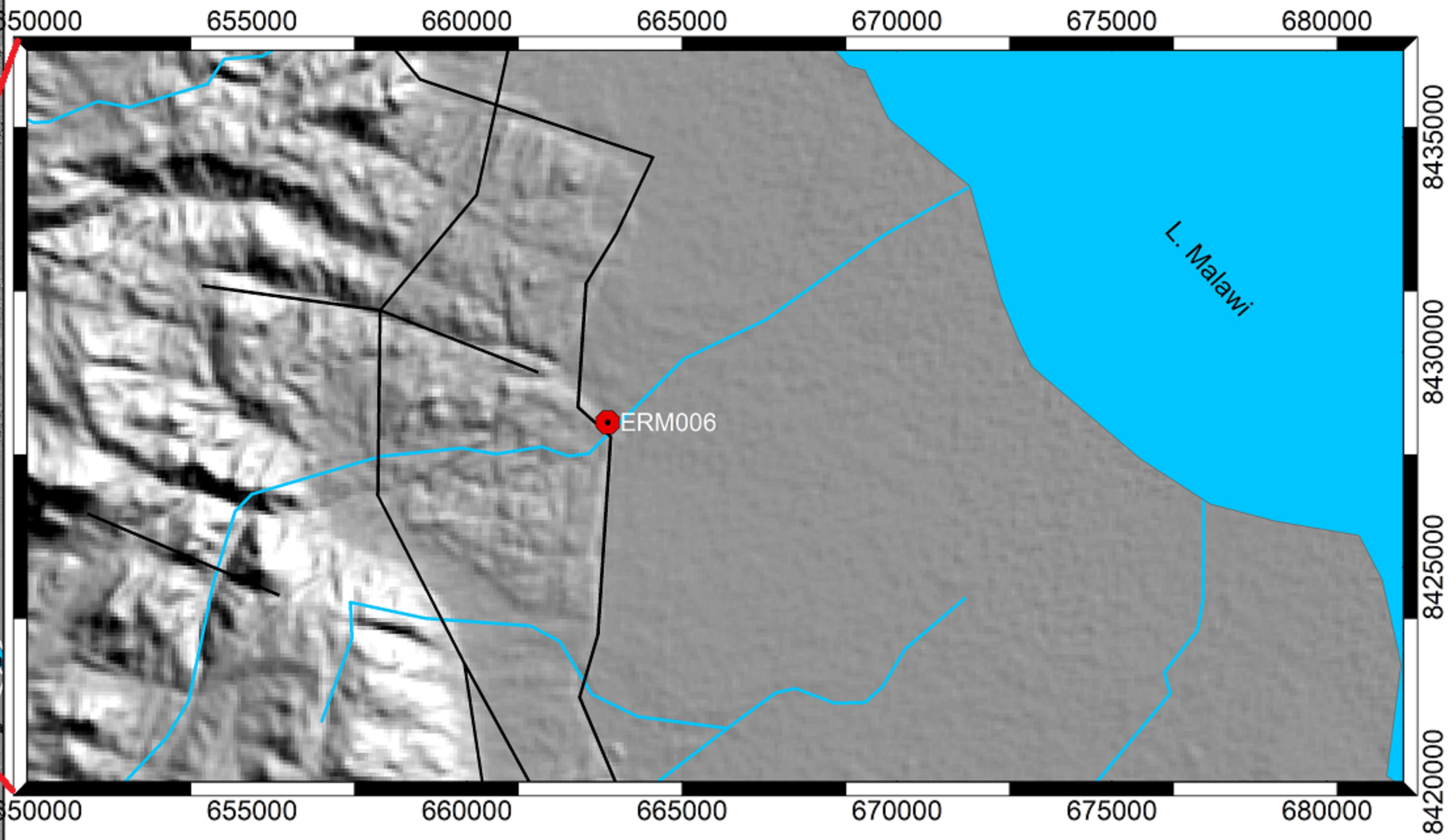
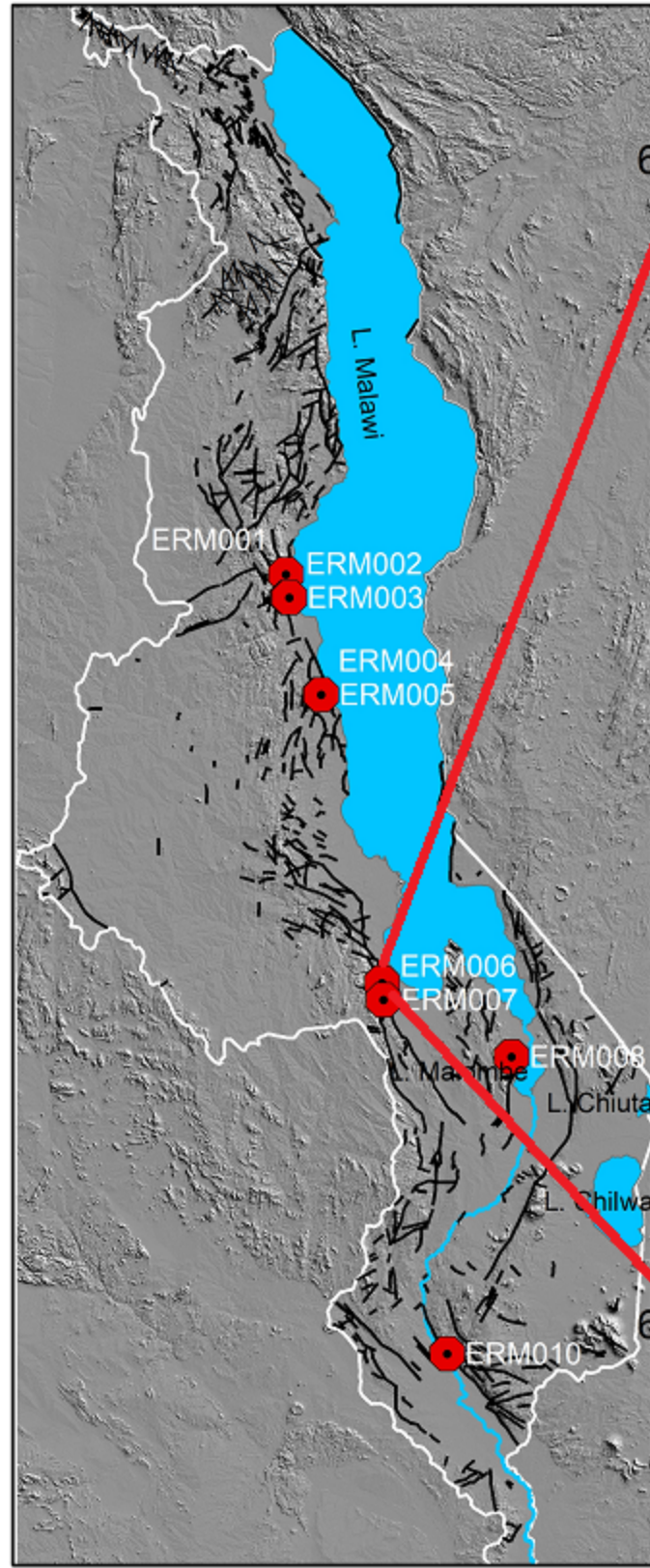


Figure 5.

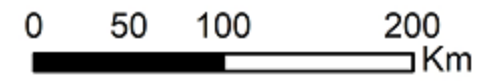
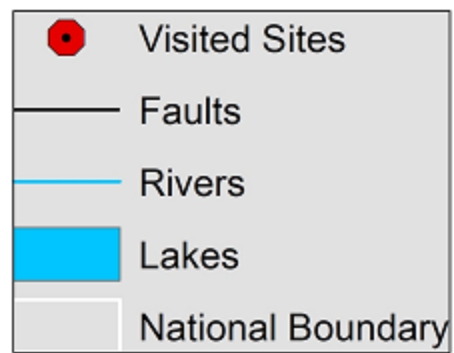
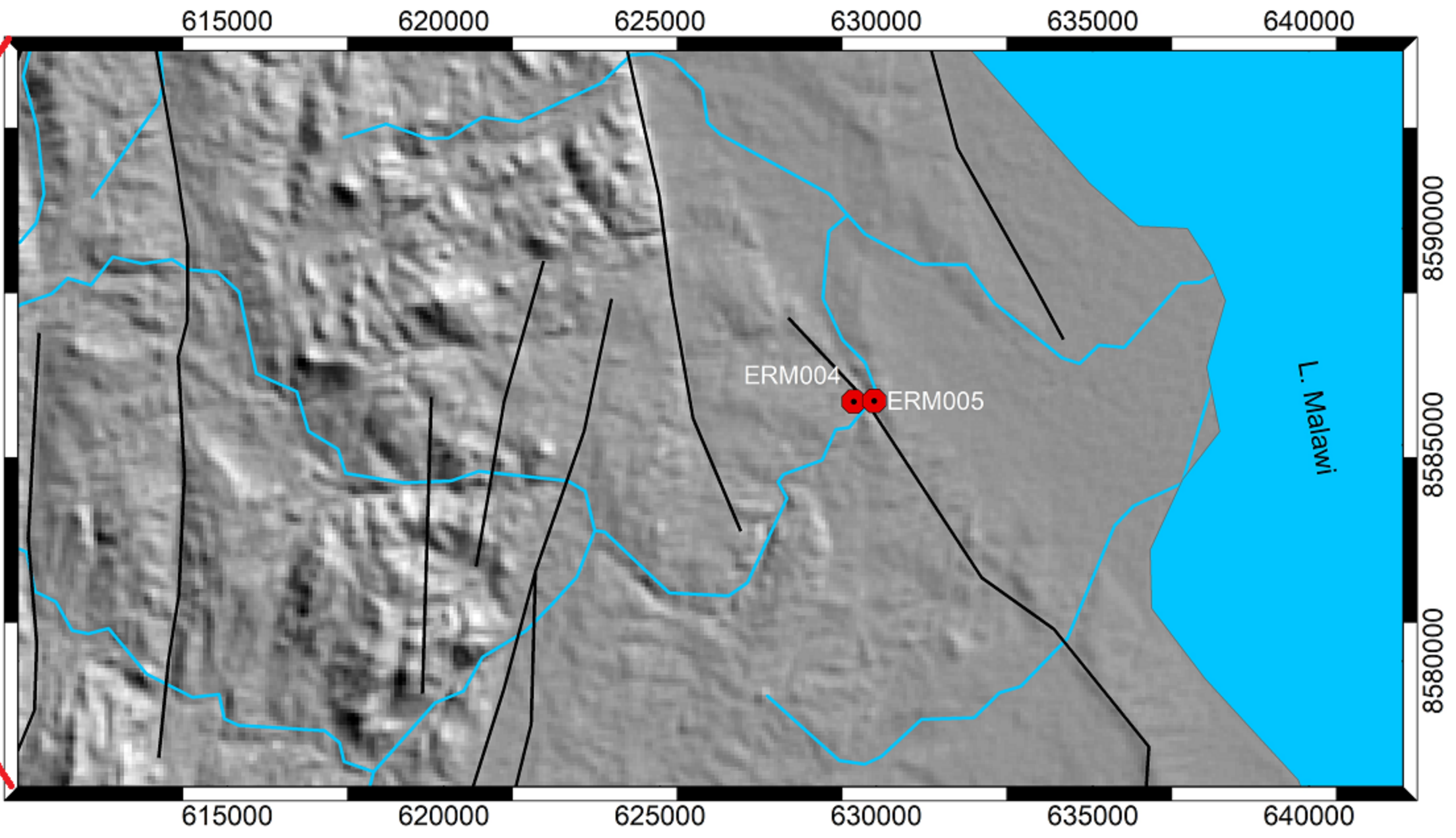
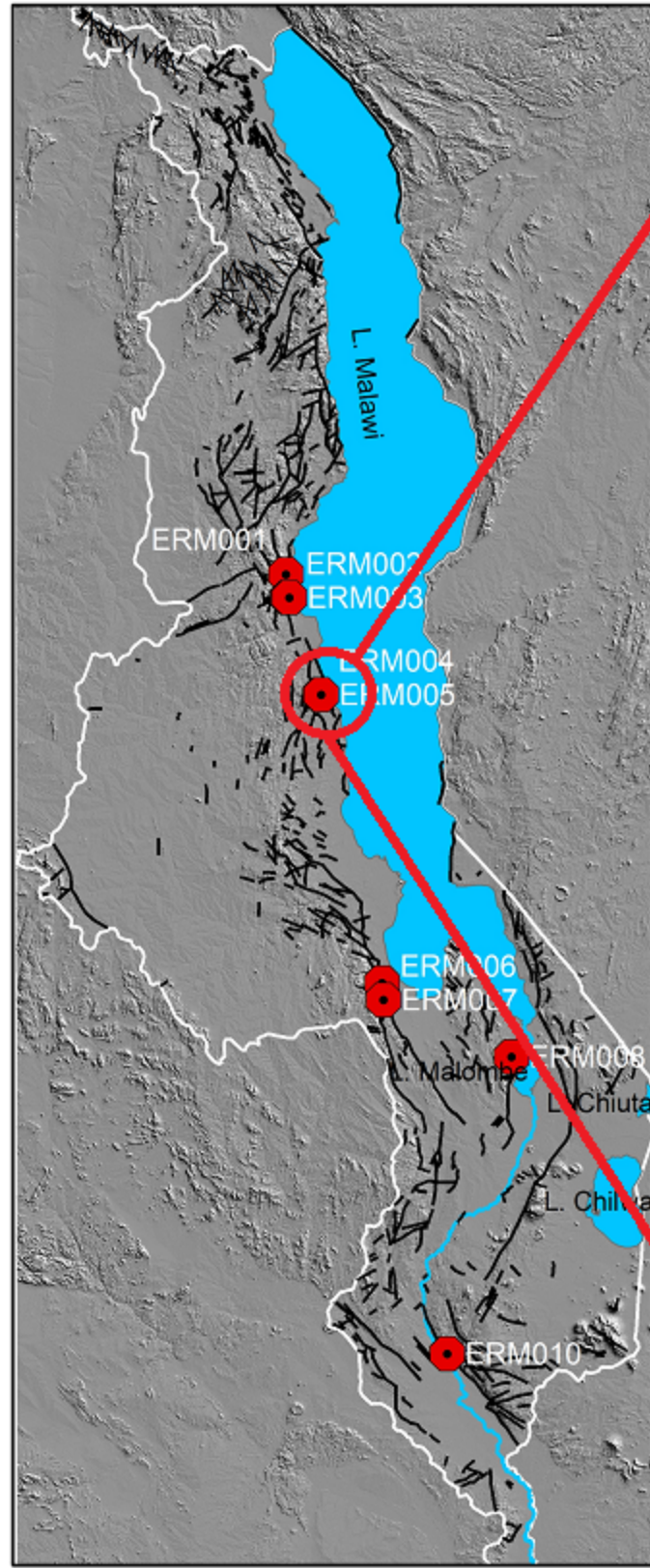


Figure 9.

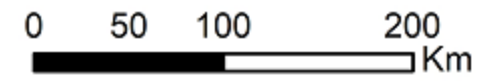
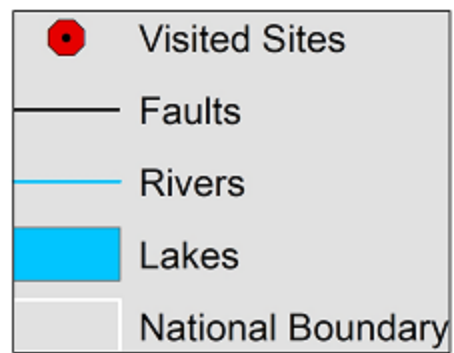
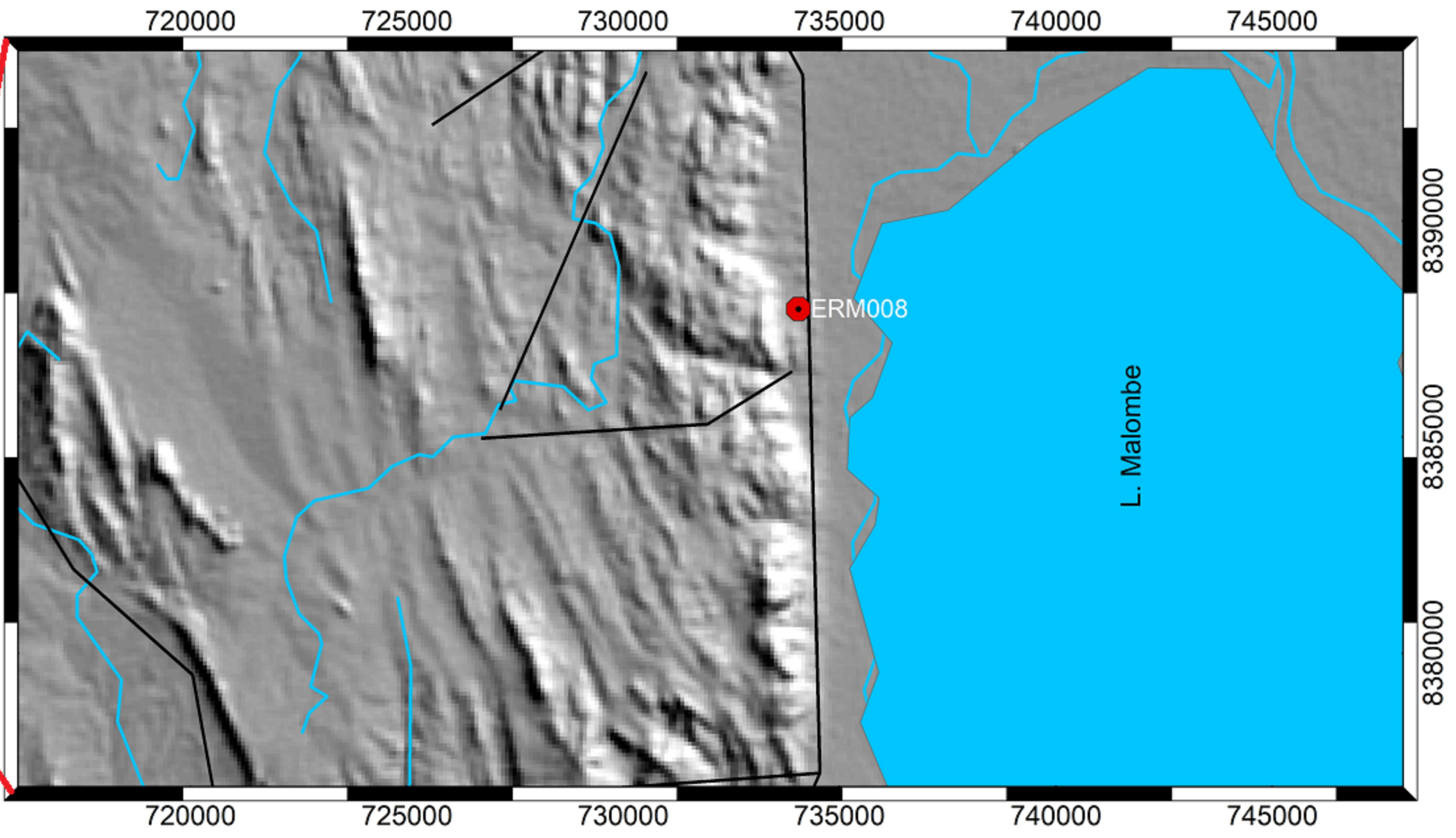
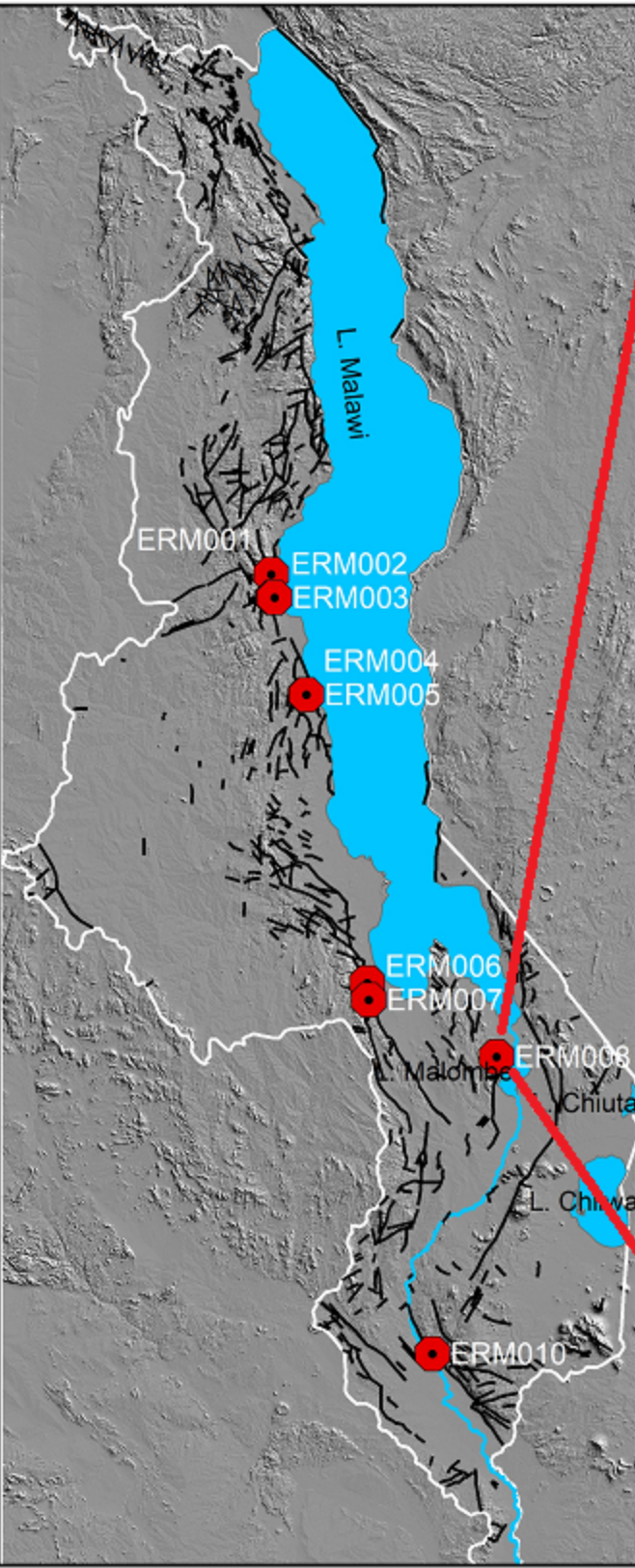


Figure 10.

